CEAI, Vol.21, No.2 pp. 43-53, 2019 Printed in Romania

Robust-Optimal Output-Voltage Control of Buck Converter using Fuzzy Adaptive Weighted Combination of Linear Feedback Controllers

Omer Saleem[1], Umar Tabrez Shami[2], Khalid Mahmood-ul-Hasan[2], Faisal Abbas[1], Samia Mahmood[1]

[1]Department of Electrical Engineering, National University of Computer and Emerging Sciences, Lahore, Pakistan (e-mail: omer.saleem, abbas.faisal, samia.mahmood@nu.edu.pk)
[2]Department of Electrical Engineering, University of Engineering and Technology, Lahore, Pakistan (e-mail: utshami@uet.edu.pk, kmhasan@uet.edu.pk)

Abstract: This paper presents a computationally-intelligent adaptive weighted controller combination scheme to optimize the output-voltage regulation capability of a low power DC-DC buck converter. The proposed scheme beneficially combines two linear feedback controllers, namely, Proportional-Integral-Derivative (PID) controller and Linear-Quadratic-Regulator (LQR). The PID controller provides control effort based on the error-dynamics of output-voltage. Wherein, the term regarding the error-derivative is replaced with the information of capacitor-current to nullify the effects of noise injected by the derivative action during transients. The LQR provides optimal control decisions by utilizing the state-feedback of inductor-current and output-voltage. The outputs of PID controller and LQR are linearly combined by computing their weighted sum. The fixed weightages associated with each controller cannot compensate the parametric uncertainties and load-step transients. Therefore, the weightages are adaptively self-tuned via a hyperbolic tangent function of error in output-voltage. The performance of weighted control scheme is also investigated by augmenting it with a fuzzy inference system that directly captures the variations in output-voltage and capacitor-current to adaptively self-tune the weightages. The performances of aforementioned weighted controllers are comparatively analyzed via credible real-time experiments. The fuzzy weighted controller yields time-optimal control effort during step-reference tracking and offers minimum-time transient recovery during load variations.

Keywords: DC-DC buck converter, linear quadratic regulator, proportional-integral-derivative controller, adaptive weighted control, fuzzy inference system.

1. INTRODUCTION

The buck converters are the main component of DC-DC power conversion systems. Together, with other constituent blocks, they are used to construct switching power supplies. They are responsible for stepping-down and regulating an input DC voltage signal at a desired level, even under the influence of load-impedance variations or input-voltage fluctuations (Tahri et al., 2012). They are mainly used in computer systems, DC machine drives, communication equipment, solar photovoltaic systems, and battery chargers due to their low power consumption and high efficiency (Ghosh and Banerjee, 2015; Akter et al., 2015).

Extensive research has been done to synthesize robust and optimal feedback controllers to further enhance the voltage regulation performance of the buck converters (Bratcu et al., 2008; Guo et al., 2009; Mariethoz et al., 2010; Lakshmi and Raja, 2014; Lindiya et al, 2015; Lee et al., 2016; Du et al., 2017; Batouba e al., 2017; Hossain et al., 2018). The buck converter uses a high-frequency switch to reduce the DC component of voltage to the required level. In addition, it consists of an inductor-capacitor filter that removes the undesired harmonics form the output-voltage signal (Rashid, 2009). The buck converter is a bilinear system that presents a different linear circuit topology during the on-state and off-state of the switch, in each time-period (Olalla et al., 2011). This periodic change in the circuit configuration leads to a discontinuous behavior in the converters. Such variable structure systems are generally controlled with the aid of Sliding-Mode-Controllers (SMCs), wherein, the switching device is operated to track a given sliding surface in the phase space (Guldemir, 2011; Ling et al, 2016). The SMCs offer robust control effort and compensate the effects of nonlinearities associated with the system (Naik and Mehta, 2017). However, the superior performance of the SMCs comes at a cost of significant control energy (Dastidar, 2010). The SMCs tend to inject chattering in the system that may result in the premature wear and tear of the switching device (Utkin and Lee, 2006). The computational synthesis of a well-postulated SMC is quite cumbersome.

The linear feedback controllers have also been rigorously investigated by the researchers to effectively control the output of buck converters (Pedroso et al., 2013a). The linear controllers, either model-free or model-based, can be easily synthesized. Owing to their shortcomings in handling nonlinear and complex dynamical electro-mechanical systems, a lot of research has been done to improve their robustness by augmenting them with additional tools. The Linear-Quadratic-Regulator (LQR) and Proportional-Integral-Derivative (PID) controllers are the most widely used buck converter controllers (Moreira et al., 2011; Hernandez et al., 2016; Debra et al., 2007, Chang et al., 2017). When individually used, each of these schemes offers certain advantages and disadvantages (Yaseen, 2017). The LQR delivers optimal control decision by minimizing a quadratic cost function that directly captures the deviations occurring in the state trajectories and control effort (Abbas et al., 2010). Once the averaged mathematical model of the system is correctly identified, the optimal state-feedback gain vector can be easily computed offline using the Algebraic Riccati Equation (Lindiya et al., 2016). Although the LQR does not directly depend on the error-dynamics, the quadratic cost function delivers a large control effort for a small change occurring in the state-trajectories, which is quite beneficial in improving the transient recovery and error convergence-rate of the response. However, it yields poor steady-state performance and exhibits significant overshoots in the response (Saleem and Omer, 2017). The LQRs are also prone to be affected by the modeling errors. On the contrary, the PID controller is a model-free scheme (Anbarasi and Muralidharan, 2016). It is the weighted sum of error, time-integral of error, and time-derivative of error (Jalilvand et al., 2010; Seshagiri et al., 2016). Despite its simple structure, it yields an effective and robust control effort due to its dependence on the variation in error-dynamics. The integral action eliminates the steady-state error, damps oscillations, and suppresses the overshoots and undershoots. However, the integral damping degrades the error convergence-rate of the response (Zhang et al., 2017). The slow response-times can be improved by introducing error-derivative control term. The derivative action improves the transitional times of the response and offers crude error-prediction based on the gradient of the error variations (Shang et al., 2009). However, it also injects high-frequency noise in the system that amplifies steady-state fluctuations in the response. Despite its demerits, the importance of derivative action cannot be ignored. The error-derivative term can be retained in the PID controller by using the information of output capacitor current (Kapat and Krein, 2012a). The PID controller formulation employing capacitor current to emulate the derivative control action is denoted as Geometric-PID controller. It has been rigorously used to yield time-optimal control effort and compensate the hysteresis effect of parasitic impedances in DC-DC converters (Kapat and Krein, 2012b). This phenomenon is also verified in (Saleem et al., 2018a) that uses a linear-quadratic-tracker augmented with an adaptive capacitor-current controller to efficiently reject the influence of random disturbances in buck converters.

This research paper presents the methodical synthesis of a robust and time-optimal control scheme for output-voltage regulation of buck converters using adaptive combination of two linear feedback controllers. Linear controllers generally offer a unique set of features. Thus, a trade-off has to be made between optimality, robustness, and design flexibility while selecting a particular control scheme (Abdullah et al., 2015). By combining the PID controller and LQR, the favorable features rendered by each controller can be selectively harnessed based on system's error-dynamics (Sun and Gan, 2010). The control effort provided by individual controllers can be beneficially combined with the objective that they optimize the controller performance in time-domain, enhance robustness against bounded exogenous disturbances, offer fast load-transient recovery, and minimize the cost of control signal (Pitel and Krein, 2009, Carradini et al., 2010).

The linear combination of the PID controller and LQR has been done by computing their weighted sum to control nonlinear dynamical systems (Salim et al., 2014; Bagheri et al., 2016). However, the fixed weightages associated with each controller may not always improve the control effort as desired. The two controllers impede each other's correctional efforts under parametric uncertainties. This phenomenon renders oscillations in the system's response as it transits from transient-state to steady-state, or vice-versa. In order to overcome this problem, the weightages are updated in each sampling interval via an online adaptation mechanism (Pedroso et al., 2013b; Saleem and Mahmood-ul-Hasan, 2018). An adaptive weighted control scheme is presented in (Pedroso et al., 2013c) that uses a Hyperbolic-Tangent-Function (HTF) of error to dynamically adjust the weightages, and hence the contribution offered by the PID controller and LQR, in each sampling interval. The proposed scheme significantly improves the time-domain response and disturbance rejection capability of the system. The weighted collaboration scheme can be further synergized by using a more elaborate set of pre-defined rules that could aid in compensating the nonlinear dynamics of the system. The desired objectives can be achieved by augmenting the online adaptation mechanism with computational intelligence techniques (Nizami and Mahanta, 2016; Lian et al., 2017). In this research, a well-postulated Fuzzy-Inference-System (FIS) is also investigated as an online adaptation mechanism for the dynamic adjustment of weightages (Salam et al., 2011; Ang et al., 2017; Saleem et al., 2017). The proposed system captures the variations in output-voltage and capacitor-current, in conjunction with a carefully orchestrated fuzzy rule-base, to render time-optimal reference tracking performance and enhanced disturbance-attenuation capability under load-transient conditions in the system.

The rest of the paper is organized as follows: Section 2 describes the experimental setup of buck converter. The theoretical background of PID controller and LQR is presented in Section 3. The synthesis of HTF and FIS based adaptive weighted control schemes are discussed in Section 4. The detailed real-time experimental analysis is presented in Section 5. The paper is concluded in the Section 6.

2. EXPERIMENTAL SETUP

The buck converter transforms a higher DC voltage to lower DC voltage level. The circuit diagram is shown in Fig. 1.

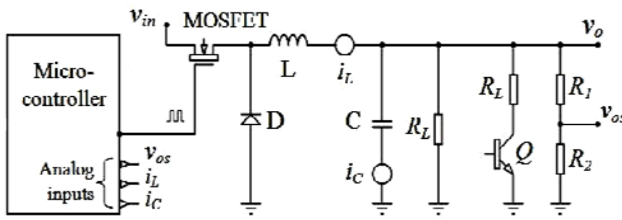

Fig. 1. DC-DC buck converter circuit.

The input voltage, v_{in}, to the circuit is passed through a high-frequency switching transistor, an N-channel MOSFET, that chops down the applied v_{in} into a rectangular waveform. The low-pass passive filter formed by the inductor-capacitor network allows only the DC component of the rectangular waveform to appear at the output. The output voltage, v_o, of the converter is given by (1). It is varied by changing the duty-cycle, d, of the MOSFET as given by (2).

$$v_o = d \times v_{in} \tag{1}$$

such that,
$$d = \frac{t_{on}}{t_{on} + t_{off}} \tag{2}$$

where, t_{on} and t_{off} refers to the on-time and off-time of switching period of MOSFET, respectively. In case of any unprecedented changes in the load-resistance, R_L, or v_{in}, the controller appropriately changes the duty-cycle of the switching period in order to maintain the v_o at the reference value. The diode, D, is reverse-biased during the on-time of switch. Thus, the entire input current is supplied to the capacitor, C, and R_L via the inductor, L. In addition, the current charges L as well. During the off-time of switch, the input current supply from the source to the circuit is cut-off. Hence, L utilizes its stored energy to supply the current to C and R_L. The diode stays forward-biased and completes the circuit during the off-time. Prior to the complete discharging of L, the MOSFET is turned-on again (Rashid, 2009). The system's hardware setup and mathematical model are presented in the following sub-sections.

2.1 Hardware Setup

The programmable buck converter module, used for experimentation, is shown in Fig. 2. The state-variables, i_L (inductor-current) and v_o, are measured in real-time using on-board current-sensing resistor of 0.01 Ω (less than the value of inductor's Equivalent-Series-Resistance) and voltage-divider circuit, formed by R_1 and R_2, respectively. An 8-bit embedded microcontroller, ATMEGA-328, acts as a relay to serially communicate sensor-measurements and control-signals between the buck converter circuit and the control system software.

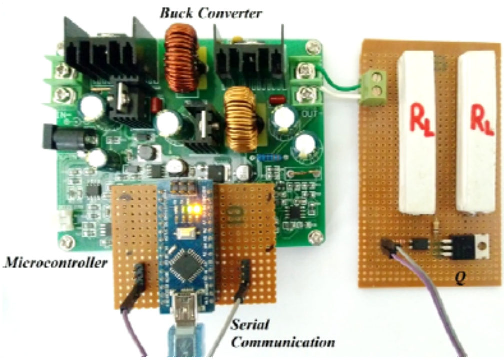

Fig. 2. Experimental setup.

The microcontroller acquires and digitizes the analog sensor-readings via its analog input channels. The sensor-readings are sampled at 250 Hz. The microcontroller serially transmits the acquired sensor data, at 9600 bps, to the control algorithm that is implemented in a LabVIEW based computer application (Demirtas and Gezer, 2010) that is running on a 64-bit, 1.2 GHz personal computer. The application graphically represents the variations in v_o in real-time and generates appropriate control commands. These commands are serially transmitted to the embedded microcontroller that converts them into high-frequency Pulse-Width-Modulated (PWM) signals, $d(t)$. A switching frequency of 150 kHz is used in this research. The PWM signals are applied to the MOSFET (IRF540N) via a dedicated driver circuit. The driver circuit amplifies the PWM signal to turn on the MOSFET. Additionally, it optically isolates the digital control circuit from the power electronic circuit to prevent it from the inductive-kick phenomenon.

The circuit also consists of a Cyclically-Switched-Resistance (CSR) that is connected in parallel with R_L. The CSR consists of a resistor identical to R_L connected in series with an NPN power bipolar junction transistor (TIP122). This transistor is denoted as Q in Fig. 1 and Fig. 2. The transistor Q remains "turned-on" under normal conditions, leading to an overall load-resistance of $0.5R_L$. When the transistor Q is turned-off, it introduces an incremental load-step transient in the response of v_o, and vice-versa. A regulated 15.0 V DC signal is applied as v_{in} to the circuit.

2.2 Mathematical Model

The state-space model of a linear dynamical system is given by (3) and (4).

$$\dot{x}(t) = \boldsymbol{A}x(t) + \boldsymbol{B}u(t) \tag{3}$$

$$y(t) = \boldsymbol{C}x(t) + \boldsymbol{D}u(t) \tag{4}$$

where, $x(t)$ is the state-vector, $y(t)$ is the output-vector, $u(t)$ is the control input signal, $\boldsymbol{A}$ is the system matrix, $\boldsymbol{B}$ is the input matrix, $\boldsymbol{C}$ is the output matrix, and $\boldsymbol{D}$ is the feed-forward matrix. The vectors, $x(t)$ and $u(t)$, are given by (5).

$$x(t) = [v_o(t) \quad i_L(t)]^T, \qquad u(t) = d(t) \tag{5}$$

where, $d(t)$ is the instantaneous value of duty-cycle. Correspondingly, the matrices $\boldsymbol{A}$, $\boldsymbol{B}$, $\boldsymbol{C}$, and $\boldsymbol{D}$ of the buck converter's state-space model are identified in (6), (Priewasser et al., 2014, Saleem et al., 2018a).

$$\boldsymbol{A} = \begin{bmatrix} -\dfrac{1}{C(0.5R_L + r_c)} & \dfrac{0.5R_L}{C(0.5R_L + r_c)} \\ -\dfrac{0.5R_L}{L(0.5R_L + r_c)} & -\dfrac{(r_L + r_c \| 0.5R_L)}{L} \end{bmatrix}, \qquad \boldsymbol{B} = \begin{bmatrix} 0 \\ \dfrac{v_{in}}{L} \end{bmatrix},$$

$$\boldsymbol{C} = [1 \quad 0], \qquad \boldsymbol{D} = 0 \tag{6}$$

The design parameters of the DC-DC buck converter used in this research are identified in Table 1.

3. THEORETICAL BACKGROUND OF EXISTING CONTROLLERS

This section presents the theoretical background of the individual control schemes.

Table 1. Design parameters of buck-converter circuit.

Parameters	Symbol	Values
Voltage divider resistance	R_1, R_2	150 kΩ
Load resistance	R_L	22 Ω
Inductance	L	330 μH
Capacitance	C	1000 μF
Equivalent-Series-Resistance (ESR) of capacitor	r_c	0.08 Ω
Equivalent-Series-Resistance (ESR) of inductor	r_L	0.05 Ω

3.1 PID Controller

The PID controllers are widely used in control industry due to their simple structure and ability to deliver effective control effort (Bhatti et al., 2015; Astom and Hagglund, 2016). The PID controller is a weighted linear combination of error, integral-of-error, and derivative-of-error (or v_o, since v_{ref} is constant). The PID control law and the error are expressed in (7) and (8), respectively.

$$u_{pid}(t) = k_p e(t) + k_i \left(\int_0^{\tau} e(\tau)\, d\tau \right) - k_d \left(\dot{v_o}(t) \right) \tag{7}$$

$$e(t) = v_{ref} - v_o(t) \tag{8}$$

The weightages of the aforementioned error-dynamics are referred to as the proportional gain (k_p), integral gain (k_i), and derivative gain (k_d), respectively. In this research, the PID gains are heuristically tuned by minimizing the Integral-Time-Absolute-Error (ITAE) criterion, shown in (9), (Vijaykumar and Manigandan, 2016; Taha et al., 2018).

$$J_1 = \int_0^{\tau} \tau |e(\tau)|\, d\tau \tag{9}$$

The heuristically optimized values of k_p, k_i, and k_d used in this research are 1.79 V^{-1}, 8.68 $(Vs)^{-1}$, and 2.49×10^{-6} sV^{-1}, respectively. The integral action in the PID control law serves to eliminate the steady-state error and damps the oscillation or overshoots caused by the transients or random perturbations in the system. However, it slows down the response as well. The derivative action is usually added in the control law to improve the system's phase margin and asymptotic convergence (Saleem et al., 2018b). However, the derivative control significantly amplifies (and injects) the high frequency noise signals to the closed-loop system. Additionally, the practical parasitic impedance(s), such as the ESR and ESL, of the capacitor further limit the performance of the derivative control term in PID controller. These parasitic impedances introduce large overshoots (and undershoots) during large-signal transients, and discrete jumps at switching transitions with alternating polarities during small-signal transients or steady-state. In order to solve these problems, a geometric formulation of PID controller is derived (Kapat and Krein, 2012a). The Geometric-PID controller replaces the $\dot{v_o}(t)$ term in the control law with the instantaneous information of the capacitor current, i_c, (Kapat and Krein, 2012b). The Geometric-PID formula uses the state-feedback of v_o and i_c. The practical model of the output capacitor is given by (10).

$$\dot{v_o}(t) = L_c \frac{d^2 i_c(t)}{dt^2} + r_c \frac{d i_c(t)}{dt} + \frac{i_c(t)}{C} \tag{10}$$

where, L_c is the Equivalent-Series-Inductance (ESL) of capacitor. Its value is 100 nH. With the inclusion of random disturbances in the capacitor model, the capacitor current of the buck converter is expressed according to (11).

$$i_c(t) \approx \frac{r_c}{r_c C - L_c} \left(e^{\frac{-t}{r_c C}} - e^{\frac{-r_c t}{L_c}} \right) C\left(\dot{v_o}(t) \right) \tag{11}$$

If the values of parasitic impedances, ESR and ESL, are considered negligibly small, then the capacitor current becomes equal to $C\left(\dot{v_o}(t)\right)$. Consequently, the Geometric-PID control law is given by (12).

$$u_{pid}(t) = k_p e(t) + k_i \left(\int_0^{\tau} e(\tau)\, d\tau \right) - \frac{k_d}{C} i_c(t) \tag{12}$$

The instantaneous value of i_c is measured by using a current-sensing resistor of 0.01 Ω (less than the value of capacitor's ESR). The usage of i_c has following benefits. Its effect on the closed-loop bandwidth and stability is insignificant (Kapat and Krein, 2012a, Saleem et al., 2018a). The i_c neither shows any overshoots nor any discrete jumps during steady-state. It also feeds forward the variations in the load-current and i_L.

3.2 Linear Quadratic Regulator

The LQR is an optimal controller that uses the linear state-space model of the dynamical system along with the full state-feedback of the system to deliver optimal control decisions (Lewis et al., 2012). It achieves this optimality by minimizing a quadratic performance index, given by (13).

$$J_2 = \int_0^{t} x^T(\tau) \boldsymbol{M} x(\tau) + u^T(\tau) \boldsymbol{R} u(\tau)\, d\tau \tag{13}$$

where, the $\boldsymbol{M}$ and $\boldsymbol{R}$ are the state- and control-penalty matrices, respectively. These matrices are chosen such that $\boldsymbol{M}$ is positive semi-definite and $\boldsymbol{R}$ is positive definite. In this research, the $\boldsymbol{M}$ and $\boldsymbol{R}$ matrices are tuned by minimizing the ITAE criterion shown in (9). The resulting matrices are expressed in (14).

$$\boldsymbol{M} = \begin{bmatrix} 4.81 \times 10^6 & 0 \\ 0 & 3.37 \times 10^7 \end{bmatrix}, \qquad \boldsymbol{R} = 100 \tag{14}$$

The state-feedback control law used to generate the optimal control commands is given by (15).

$$u_{lqr}(t) = -\boldsymbol{K} x(t) \tag{15}$$

where, $\boldsymbol{K}$ is denoted as the state-feedback gain vector. The gain vector relocates the poles of the system to synthesize an optimal controller. The state-feedback gain vector, $\boldsymbol{K}$, is given by (16).

$$\boldsymbol{K} = \boldsymbol{R}^{-1} \boldsymbol{B}^T \boldsymbol{P} \tag{16}$$

where, **P** is a symmetric positive definite matrix that is evaluated using the Algebraic Riccati Equation, as shown in (17).

$$\boldsymbol{A}^T \boldsymbol{P} + \boldsymbol{P}\boldsymbol{A} - \boldsymbol{P}\boldsymbol{B}\boldsymbol{R}^{-1}\boldsymbol{B}^T\boldsymbol{P} + \boldsymbol{M} = 0 \tag{17}$$

According to the performance index, the applied control signal is proportional to the square of state variations. Thus, if the variations are large, the minimization is faster and the LQR system converges quickly to deliver an optimal gain vector. Consequently, the transition time of the response and error convergence improves significantly while utilizing minimum energy. The optimal gain vector is evaluated offline using the expression given (16). The evaluated gain vector is given by (18).

$$\boldsymbol{K} = [165.93 \quad 579.68] \tag{18}$$

4. WEIGHTED CONTROLLER COMBINATION SCHEME

Owing to their design limitations, each of the aforementioned linear control schemes offer unique attributes in controlling v_o of the buck converter. Individually, they are capable of enhancing only a few performance parameters. Thus, the two control schemes are beneficially combined by taking their weighted sum, as shown in (19), in order to fulfill the desired control objectives.

$$u(t) = w \times u_{lqr}(t) + (1 - w) \times u_{pid}(t) \tag{19}$$

where, w is the weightage, such that $w \in [0, 1]$.

4.1 Fixed Weighted Controller (f-WC)

Initially, the fixed value of w is tuned by minimizing the ITAE criterion given in (9). The value of w thus selected is 0.659. This controller variant is denoted as the fixed-Weighted-Controller (f-WC). The block diagram of the f-WC is shown in Fig. 3.

4.2 Adaptive Weighted Control Scheme

The controller combination can be further synergized by utilizing an adaptive weighted control mechanism.

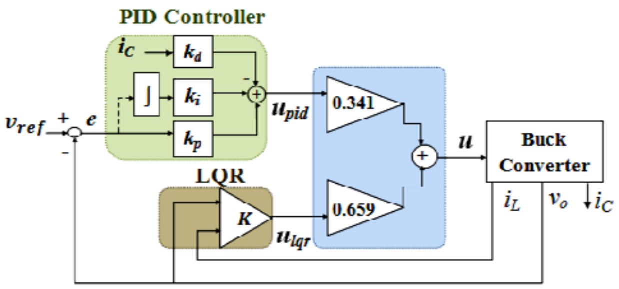

Fig. 3. Fixed Weighted Controller (f-WC).

Wherein the weightages are adaptively modulated using a pre-defined set of rules that depends on the error-dynamics of the system. The proposed scheme effectively combines the efficiencies of each controller and suppresses their deficiencies, so that only the best features of the available control resources are utilized at a given instant. Additionally, it ensures a smoother transition between the controllers. In this research, two different online adaptation mechanisms are investigated for dynamic adjustment of w, namely, HTF and FIS.

A. Hyperbolic Adaptive Weighted Controller (HAWC)

The weightages of the WSM can be automatically updated by using a nonlinear function of error in v_o, as proposed in (Pedroso et al., 2013c). The nonlinear scaling of the individual control schemes enables the overall control mechanism to quickly adapt to variations in system dynamics and improve the reference-tracking accuracy. Therefore, a smooth nonlinear function is needed to change the values of w automatically with respect to error-variations. The refined control objectives are explained as follows: If the error is large, the value of w should appropriately increase the control contribution of the LQR so that the convergence-rate of the response is significantly improved. For smaller errors (as the response approaches the reference voltage), the PID controller contribution should be increased so that the steady-state fluctuations are eliminated and the oscillations (or overshoots) are suppressed.

Several nonlinear scaling functions have been proposed in the literature, such as, Gaussian Functions (GF), Piecewise Linear Functions (PLF), and HTF, etc (Seraji, 1998). The symmetrical GFs contain a number of hyper-parameters that have to be either experimentally or algorithmically optimized, which is a cumbersome process (Pedroso et al., 2013a). Despite their robustness, the PLFs are quite difficult to construct. The dynamic variations occurring in the systems must be accurately identified for optimal construction of a piecewise control surface. The HTF is a simple, symmetrical, and differentiable smooth sigmoidal function. The smooth and gradual increment of the waveform, with respect to error-dynamics, leads to a smoother transition between the controllers and thus eliminates the chattering phenomenon. It can be restricted between 0 and 1 by taking the absolute value of the error-variable. It does not put any recursive computational burden on the digital signal processor because of its straight-forward algorithmic implementation.

Due to the aforementioned characteristics, the HTF has been chosen for adaptive collaboration of the two controllers in (Pedroso et al., 2013c). The HTF used for adaptive self-tuning for w in this research is given by (20).

$$w = tanh\,|e(t)| \tag{20}$$

The waveform of HTF is shown in Fig. 4. The expression in (20) does not contain any hyper-parameter to be optimized. The control system architecture of the Hyperbolic Adaptive Weighted Controller (HAWC) is illustrated in Fig. 5.

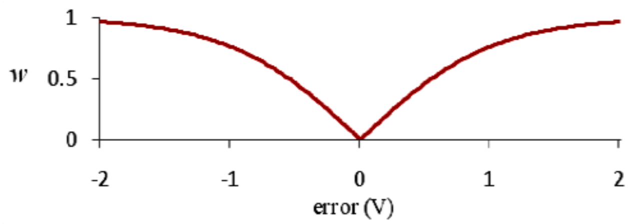

Fig. 4. Waveform of HTF.

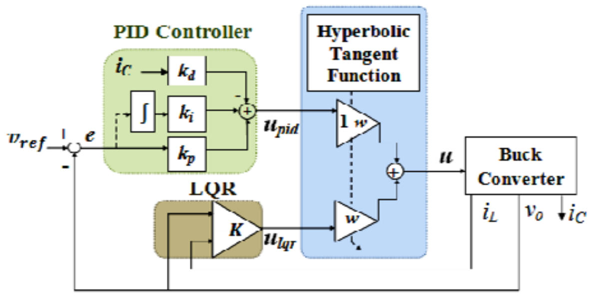

Fig. 5. Hyperbolic Adaptive Weighted Controller (HAWC).

Owing to its computational efficiency and simple construction, the HAWC is a practicable control scheme for real-time applications. However the simplicity of HTF comes at a cost. Due to a single degree-of-freedom, the adaptation mechanism is not flexible enough to address the unprecedented nonlinearities and complexities occurring in switching converters in real time.

B. Fuzzy Adaptive Weighted Controller (FAWC)

The HTF-based adaptive tuning mechanism depends solely on the error variable. Hence, it does not ensure efficient commutation between the two linear controllers in order to effectively handle unprecedented dynamic variations occurring in the system. To further enhance the controller's performance, a two-input and one-output Fuzzy-Inference-System (FIS) is employed for the real-time self-tuning of w.

The FIS is a linguistic model-free technique that resembles the human-decision making process to deduce optimal solutions for complex engineering problems. In this research, it is utilized to intelligently adjust the value of w according to a set of heuristically synthesized qualitative logical (if-then-else) rules, after every sampling interval (Lian et al., 2006; Martinez et al., 2012; Mahendran et al., 2016). The fuzzy rule-base is carefully synthesized in order to include correctional efforts regarding various control scenarios emerging in the system. Hence, a two-dimensional Toeplitz rule-base is empirically defined to optimally adjust the value of w and hence, derive robust control decisions after each sampling interval. Unlike the HTF adaptation mechanism proposed in (Pedroso et al., 2013c), the pre-defined logical rule base of FIS depends on two input state-variables, $e(t)$ and $i_c(t)$. The inclusion of $e(t)$ and $i_c(t)$ in the fuzzy rule-base increases the degrees-of-freedom of the controller as well as the flexibility of controller design. This feature allows for stable transition of the closed-loop system between the constituent controllers under parametric uncertainties. Additionally, it enables the control scheme to compensate even those intrinsic nonlinear disturbances that could not be rejected via the HTF-based adaptive weighted controller. The information of error-derivative, or $i_c(t)$, in conjunction with the elaborate fuzzy rules helps in minimizing the convergence-time during load transients, followed by damping of oscillations to allow for a smoother settling. This phenomenon enhances the time-optimal control effort of the system as well as its robustness against the bounded exogenous disturbances. The process of fuzzification and defuzzification does not put any computational burden on the digital computer used in this research, which makes this technique practically implementable in real-time.

The functionality of the FIS is presented as follows. First of all, the input signals are normalized between -1 and 1. The normalized input signals are fuzzified into linguistic variables. The linguistic variables of input membership functions (MF), for e and i_c, are defined as: Negative-Big (NB), Negative-Medium (NM), Negative-Small (NS), Zero (Z), Positive-Small (PS), Positive-Medium (PM), and Positive-Big (PB). Hence, there a total of 49 rules. The linguistic variables of the output MF are defined as: Zero (Z), Small (S), Medium (M), Big (B), and Very-Big (VB). The rule-base is presented in Table 2. After the fuzzification of the inputs, the implication method is applied followed by the aggregation of the fuzzy outputs using the maximum-minimum fuzzy inference technique, as shown in (21).

$$\mu_i = min\big(f_i(\hat{e}), f_i(\hat{i_c})\big) \tag{21}$$

where, μ is the grade-value of MF, $f(x)$ is the triangular MF, i is the number of rule, and $\hat{e}$ and $\hat{i_c}$ are the normalized values of e and i_c, respectively. The triangular MF, $f(x)$, is given by (22).

$$f_i(x) = \begin{cases} 1 + \dfrac{x - c_i}{{b_i}^-}, & -{b_i}^- \le x - c_i \le 0 \\ 1 - \dfrac{x - c_i}{{b_i}^+}, & 0 \le x - c_i \le {b_i}^+ \\ 0, & otherwise \end{cases} \tag{22}$$

where, b_i^-, c_i, and b_i^+ are the left-half width, center, and right-half width of the MF, respectively. The waveforms of the input and output MF are shown in Fig. 6 and 7, respecively.

Table 2. Fuzzy Rule-Base for Adaptive Self-tuning of Weightage.

w		i_c						
		NB	NM	NS	Z	PS	PM	PB
e	NB	VB	VB	B	B	B	VB	VB
	NM	VB	B	M	M	M	B	VB
	NS	B	B	M	S	M	B	B
	Z	B	M	S	S	S	M	B
	PS	B	B	M	S	M	B	B
	PM	VB	B	M	M	B	B	VB
	PB	VB	VB	B	B	B	VB	VB

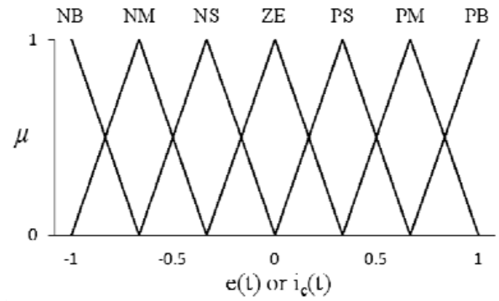

Fig. 6. Waveform of input MF.

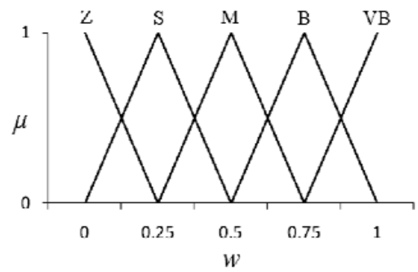

Fig. 7. Waveform of output MF.

The aggregated output fuzzy set is de-fuzzified to compute a crisp value of w via the center-of-area method, given by (23).

$$w = \frac{\sum_{i=1}^{n} \mu_i \acute{c_i}}{\sum \mu_i} \tag{23}$$

where, $\acute{c_i}$ is the center of output MF. The block diagram of Fuzzy Adaptive Weighted Controller is shown in Fig. 8.

5. TESTS AND RESULTS

The voltage regulation performance of the PID controller, LQR, f-WC, HAWC, and FAWC is tested via the following two 'hardware-in-the-loop' experiments.

Test A: The performance of the controllers in tracking a step-reference of +5.0 V is tested. The resulting variations in v_o, exhibited by each controller, are shown in Fig. 9, 10, 11, 12, and 13. The corresponding variations in w, in HAWC and FAWC, are shown in Fig. 14 and 15, respectively. The FAWC demonstrates superior reference tracking performance as compared to other controllers. It quickly converges to v_{ref} with negligible overshoot and minimal steady-state error.

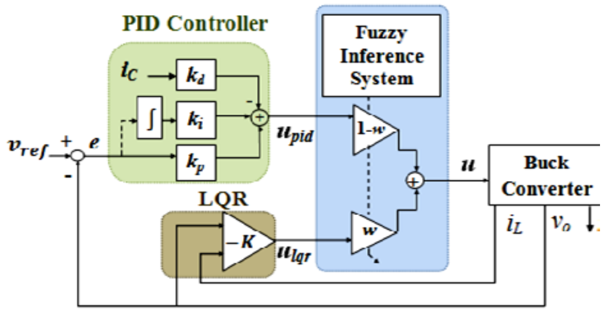

Fig. 8. Fuzzy Adaptive Weighted Controller (FAWC).

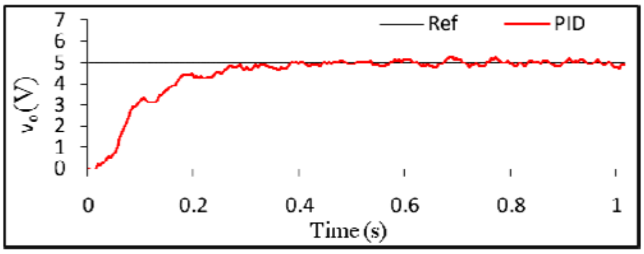

Fig. 9. Step-response exhibited by PID controller.

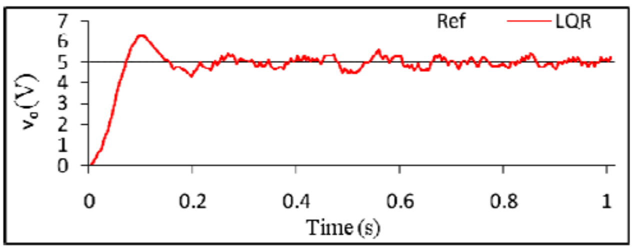

Fig. 10. Step-response exhibited by LQR.

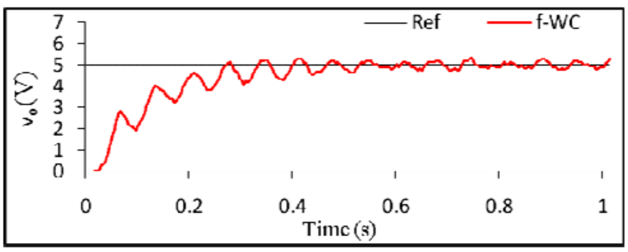

Fig. 11. Step-response exhibited by f-WC.

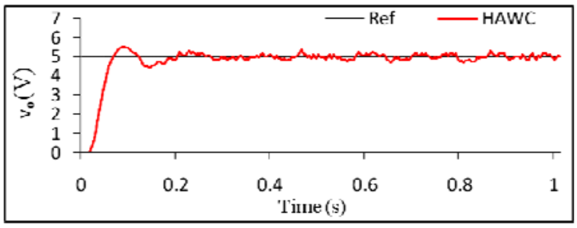

Fig. 12. Step-response exhibited by HAWC.

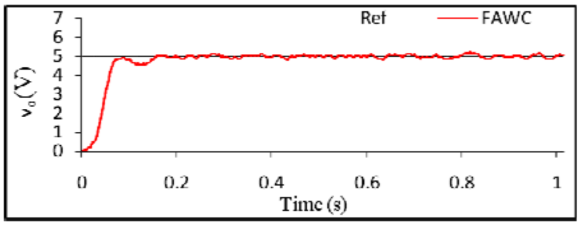

Fig. 13. Step-response exhibited by FAWC.

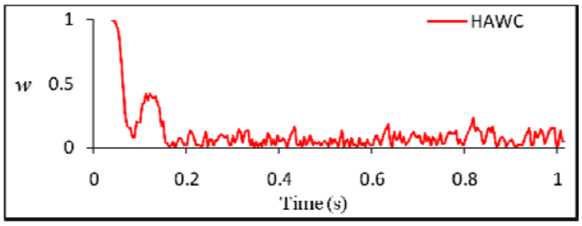

Fig. 14. Variations in 'w' for HAWC.

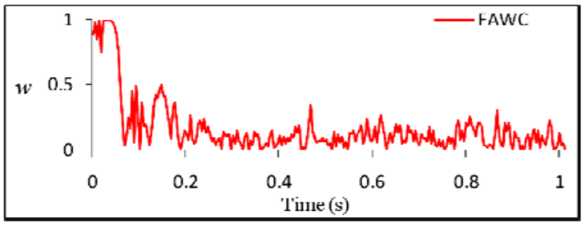

Fig. 15. Variations in 'w' for FAWC.

Test B: The voltage regulation performance of each controller is tested under load disturbance conditions. The load-step transient resembles the impulsive disturbance and modeling error (since R_L is part of the buck converter's state-space representation). The load-step transient is introduced by turning-off the transistor Q at t ≈ 1.25s. The abrupt variations exhibited by v_o for a 100% step increment in R_L are illustrated in Fig. 16, 17, 18, 19, and 20. The corresponding variations in the w for HAWC and FAWC are shown in Fig. 21 and 22, respectively.

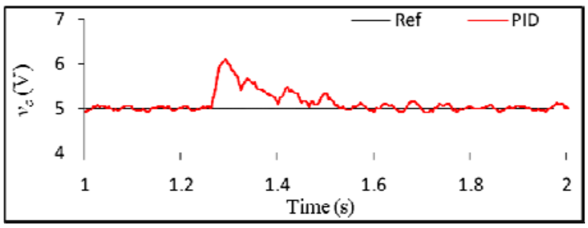

Fig. 16. Response of PID controller under load-step transient.

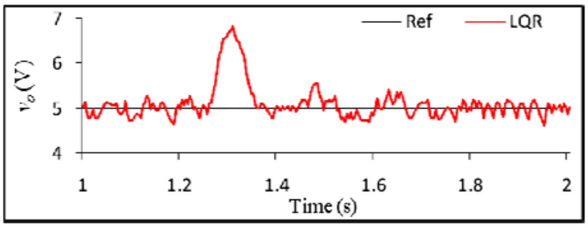

Fig. 17. Response of LQR under load-step transient.

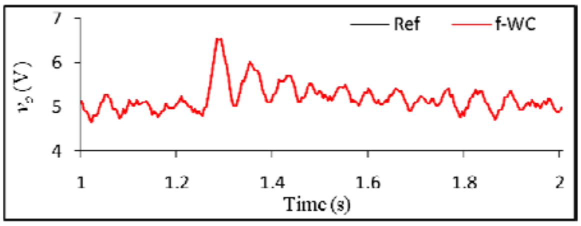

Fig. 18. Response of f-WC under load-step transient.

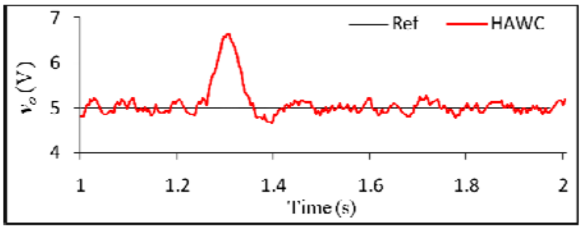

Fig. 19. Response of HAWC under load-step transient.

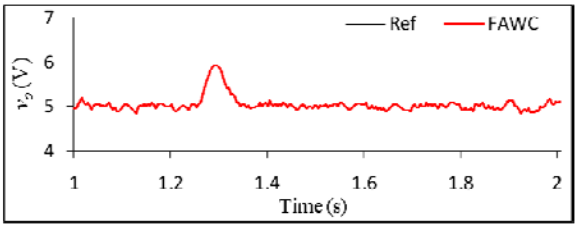

Fig. 20. Response of FAWC under load-step transient.

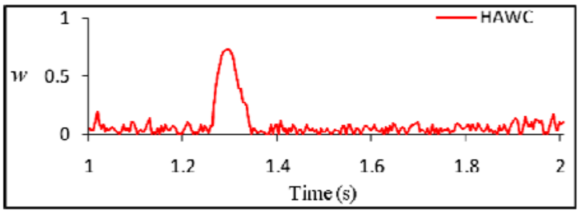

Fig. 21. Variations in 'w' for HAWC under load-step transient.

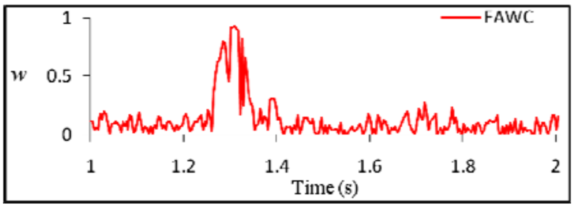

Fig. 22. Variations in 'w' for FAWC under load-step transient.

The performance assessment of the results of Test-A and Test-B is summarized in Table 3. The comparison is done in terms of the rise-time (t_r), overshoot (OS), settling-time (t_s), and root-mean-squared value of steady-state error (E_{ss}) exhibited by each individual controller. The experimental perfromance of the proposed FAWC control scheme is benchmarked against the conventional PID controller, the LQR, and their adaptive collaborative variants and is found to be on par with it. The comaprison clearly validates the superiror robustness and optimality of the FAWC against the conventional control schemes. The FAWC surpasses the aforementioned (exisitng) control schemes by significantly improving the overall time-domain performance of the system.

Table 3. Summary of test results.

Controller	Test-A				Test-B	
	t_r (s)	OS (V)	t_s (s)	E_{ss} (V)	OS (V)	t_s (s)
PID	0.28	0.02	0.45	0.10	1.10	0.26
LQR	0.11	1.27	0.25	0.28	1.82	0.12
f-WC	0.24	0.08	0.51	0.22	1.53	0.41
HAWC	0.10	0.54	0.20	0.18	1.65	0.18
FAWC	0.11	0.01	0.18	0.09	0.98	0.08

In Test-A, the LQR response demonstrates the highest overshoot, where as, the PID controller exhibits the largest transitional times. The f-WC shows persistent chattering. The HAWC scheme shows considerable improvement over the PID, LQR and f-WC controller. The FAWC exhibits the most time-optimal control effort while tracking the step-reference. It renders relatively rapid transits while daming the overshoots and oscillations in the response. Similarly, in Test-B, the FAWC effectively rejects the exogenous disturbances by quickly converging the response to v_{ref} while exhibiting minimal overshoot and negligible oscillations in the response.

In both testing scenarios, the variation behavior of 'w' clearly validates that FAWC is relatively more responsive to the changes in system dynamics and hence assures considerable improvement in the response as compared to the exisitng HAWC scheme, implemented in (Pedroso et al., 2013c). Since w is fixed in the f-WC scheme, it delivers relatively poor control effort. It commutes abruptly between the two constituent controllers which causes persistent chattering in the response.

6. CONCLUSION

This paper addresses the importance of computational intelligence to improve the control performance and compensate the nonlinearities associated with a complex dynamical system, using conventional linear feedback controller. Different collaborative control mechanisms are investigated to optimize the voltage regulation of a buck converter. The LQR delivers optimal control effort by minimizing the deviations in state-trajectories and control effort. The PID controller renders improved reference-tracking capability and damps the steady-state errors caused by the parametric uncertainties and parasitic impedances. The LQR and PID controller work together to yield improved convergence-rate, time-domain response, and robustness against exogenous disturbances. Each controller variant is tested in real-time. The comparative assessment of the test-results clearly validates the superior performance of the FAWC over other controllers discussed in this research.

Unlike the HTF technique, the fuzzy inference system in FAWC uses two state-variables, e and i_c, to appropriately update w. This increases the degrees-of-freedom and flexibility of the mechanism to generate optimal control commands. In future, other intelligent self-tuning mechanisms can be investigated to further enhance the performance of weighted adaptive control schemes for DC-DC converters. Different soft-computing, meta-heuristic, and evolutionary optimization algorithms can be investigated to select the $\boldsymbol{M}$ and $\boldsymbol{R}$ weighting matrices of the quadratic cost function. The proposed adaptive control mechanism can also be tested on other DC-DC switch-mode power electronic converters, such as, boost, buck-boost, flyback, Cuk, Sepic, or Zeta converters. The Linear-Quadratic-Gaussian controllers and Fractional-Order PID controllers can also be intelligently combined and investigated to further enhance the robustness and time-optimality of the system's reference-tracking response and load-transient compensation.

REFERENCES

Abbas, G., Abouchi, N., and Pillonnet, G. (2010). Optimal State-Space Controller for Power Switching Converter. In: *2010 IEEE Asia Pacific Conference on Circuits and Systems*, Kuala Lumpur, Malaysia, pp. 867-870.

Abdullah, M.A., Tan, C.W., and Yatim, A.H.M. (2015). A Simulation Comparison of PI and Linear Quadratic Regulator Controllers in DC-DC Converter. In: *2015 IEEE Conference on Energy Conversion*, Johor Bahru, Malaysia, pp. 37-41.

Akter, P., Uddin, M., Mekhilef, S., Tan, N.M.L, and Akagi, H. (2015). Model Predictive Control of Bidirectional Isolated DC–DC Converter for Energy Conversion System. *International Journal of Electronics*, 102(8), pp. 1407-1427.

Anbarasi, S., and Muralidharan, S. (2016). Enhancing the Transient Performances and Stability of AVR System with BFOA Tuned PID Controller. *Control Engineering and Apllied Informatics*, 18(1), pp. 20-29.

Ang, G., Arcibal, P.J., Crisostomo, L.M.R., Ostia, C.F., and Tabuton, J.E.C. (2017). Implementation of a Fuzzy Controlled Buck-Boost Converter for Photovoltaic Systems. *Energy Procedia*, 143, pp. 641-648.

Astrom, K.J., and Hagglund, T. (2016). *Advanced PID Control*. Instrumentation, Systems, and Automation Society, North Carolina, USA.

Bagheri, S., Jafarovt, T., Freidovich, L., and Sepehri, N. (2016). Beneficially Combining LQR and PID to Control Longitudinal Dynamics of a Smartfly UAV. In: *2016 IEEE 7th Annual Information Technology, Electronics and Mobile Communication Conference*, Vancouver, BC, Canada, pp. 1-6.

Bhatti, O.S., Mehmood-ul-Hasan, K., and Imtiaz, M.A. (2015). Attitude Control and Stabilization of a Two-Wheeled Self-Balancing Robot. *Control Engineering and Applied Informatics*, 17(3), pp. 98-104.

Boutouba, M., El-Ougli, A., Miqoi, S., and Tidhaf, B. (2017). Intelligent Control for Voltage Regulation System via DC-DC Converter using Raspberry Pi 2 Board. *WSEAS Transactions on Electronics*, 8, pp. 41-47.

Bratcu, A.I., Munteanu, I., Bacha, S., and Raison, B. (2008). Maximum Power Point Tracking of Grid-connected Photovoltaic Arrays by Using Extremum Seeking Control. Control Engineering and Applied Informatics, 10(4), pp. 3-12.

Chang, C., Hong, C., Zhao, X., and Wu, C. (2017). An Analysis of the Limit Cycle Oscillation in Digital PID Controlled DC-DC Converters. *Journal of Power Electronics*, 17(3), pp.686-694.

Corradini, L., Babazadeh, A., Bjeletic, A., and Maksimovic, D. (2010). Current-Limited Time-Optimal Response in Digitally Controlled DC–DC Converters. *IEEE Transactions on Power Electronics*, 25(11), pp. 2869 – 2880.

Dastidar, R.G. (2010). On the Advantages and Limitations of Sliding Mode Control for Spacecraft. In: *AIAA SPACE 2010 Conference & Exposition*, Anaheim, California, pp. 1-7.

Demirtas, M., and Gezer, G. (2010). Analyzing of PI Controlled DC/DC Converter Output Voltage using LABVIEW. In: *2010 IEEE 18th Signal Processing and Communications Applications Conference,* Diyarbakir, Turkey, pp. 704-707.

Dobra, P., Trusca, M., Moga, D., and Petreus, D. (2007). Stability Aspects in DC-DC Converters using PID Controller. *Control Engineering and Applied Informatics*, 9(1), pp. 33-40.

Du, G., Liu, Z., Du, F., and Li, J. (2017). Performance Improvement of Model Predictive Control using Control Error Compensation for Power Electronic Converters Based on the Lyapunov Function. *Journal of Power Electronics,* 17(4), pp.983-990.

Ghosh, A., Banerjee, S. (2015) Control of Switched-Mode Boost Converter by using Classical and Optimized Type Controllers. *Control Engineering and Applied Informatics*, 17(4), pp. 114-125

Guldemir, H. (2011). Study of Sliding Mode Control Of DC-DC Buck Converter. *Energy and Power Engineering*, 3(4), pp. 401-406.

Guo, L., Hung, J.Y., and Nelms, R.M. (2009). Evaluation of DSP-Based PID and Fuzzy Controllers for DC–DC Converters. *IEEE Transactions on Industrial Electronics*, 56(6), pp. 2237 – 2248.

Hernandez, D.M., Diaz, V.R.G., Castellanos, J.F.G., Aguilar, G.M., and Pareschi, F. (2016). Design of Buck DC-DC Converters from the Linear Quadratic Regulator Approach. In: *2016 IEEE International Power Electronics and Motion Control Conference*, Varna, Bulgaria, pp. 952 -956.

Hossain, M.Z., Rahim, N.A., and Selvaraj, J. (2018). Recent Progress and Development on Power DC-DC Converter Topology, Control, Design And Applications: A Review. *Renewable and Sustainable Energy Reviews*, 81(1), pp. 205-230.

Jalilvand, A., Vahedi, H., and Bayat, A. (2010). Optimal Tuning of the PID Controller for a Buck Converter using

Bacterial Foraging Algorithm. In: *2010 3rd IEEE International Conference on Intelligent and Advanced Systems*, Kuala Lampur, Malaysia, pp. 1-5.

Kapat, S., and Krein, P.T. (2012). Improved Time Optimal Control of a Buck Converter Based on Capacitor Current," *IEEE Transactions on Power Electronics*, 27(3), pp. 1444-1454.

Kapat, S., and Krein, P.T. (2012). Formulation of PID Control for DC–DC Converters based on Capacitor Current: A Geometric Context. *IEEE Transactions on Power Electronics*, 27(3), pp. 1424-1432.

Lakshmi, S., and Raja, T.S.R. (2014). Design and Implementation of an Observer Controller for a Buck Converter. *Turkish Journal of Electrical Engineering and Computer Sciences*, 22(3), pp. 562-572.

Lee, B.S., Kim, S.K., Park, J.H., and Lee, K.B. (2016). Adaptive Output Voltage Tracking Controller for Uncertain DC/DC Boost Converter. *International Journal of Electronics*, 103(6), pp. 1002-1017.

Lewis, F.L., Vrabie, D., and Syrmos, V.L. (2012). *Optimal Control*. John Wiley and Sons, New Jersey, USA.

Lian, K.Y., Liou, J.J., and Huang, C.Y. (2006). LMI-based Integral Fuzzy Control Of DC-DC Converters. *IEEE Transactions of Fuzzy Systems*, 14(1), pp. 71-80.

Lian, K.Y., Liu, C.H., and Chiu, C.S. (2017). Robust Fuzzy Output Regulator Design for Nonlinear Systems without Virtual Desired Variable Calculation. *Control Engineering and Applied Informatics*, 19(1), pp. 27-36.

Lindiya, A., Palani, S., and Iyyappan. (2012). Performance Comparison of Various Controllers for DC-DC Synchronous Buck Converter. *Procedia Engineering*, 38, pp. 2679-2693.

Lindiya, S.A., Vijayarekha, K., and Palani, S. (2016). Deterministic LQR Controller for DC-DC Buck Converter. In: *2016 Biennial International Conference on Power and Energy Systems: Towards Sustainable Energy*, Bangalore, India, pp. 1-6.

Ling, R., Maksimovic, D., and Leyva, R. (2016). Second-Order Sliding-Mode Controlled Synchronous Buck DC–DC Converter. *IEEE Transactions on Power Electronics*, 31(3), pp. 2539 – 2549.

Mahendran, V., and Ramabadran, R. (2016). Fuzzy-PI-based Centralised Control of Semi-Isolated FP-SEPIC/ZETA BDC in a PV/Battery Hybrid System. *International Journal of Electronics*, 103(11), pp. 1909-1927.

Mariethoz, S., Almer, S., Baja, M., Beccuti, A.G., Patino, D., Wernrud, A., Buisson, Cormerais, J.H., Geyer, T., Fujioka, H., Jonsson, U.T., Kao, C.Y., Morari, M., Papafotiou, G., Rantzer, A., and Riedinger, P. (2010). Comparison of Hybrid Control Techniques for Buck and Boost DC-DC Converters. *IEEE Transactions on Control Systems Technology*, 18(5), pp. 1126 – 1145.

Martinez, J.S., Hissel, D., and Péra, M.C. (2012). Type-2 Fuzzy Logic Control of a DC/DC Buck Converter. *IFAC Proceedings Volumes*, 45(21), pp. 103-108.

Moreira, C.O., Silva, F.A., Pinto, S.F., and Santos, M.B. (2011). Digital LQR Control with Kalman Estimator for DC-DC Buck Converter. In: *2011 IEEE EUROCON – International Conference on Computer as a Tool*, Lisbon, Portugal, pp. 1-4.

Naik, B.B., and Mehta, A.J. (2017). Sliding Mode Controller with Modified Sliding Function for DC-DC Buck Converter. *ISA Transactions*, 70, pp. 279-287.

Nizami, T.K., and Mahanta, C. (2016). An Intelligent Adaptive Control of DC–DC Buck Converters. *Journal of the Franklin Institute*, 353(12), pp. 2588-2613.

Olalla, C., Queinnec, I., Leyva, R., Aroudi, A.E. (2011). Robust Optimal Control of Bilinear DC–DC Converters. *Control Engineering Practice*, 19(7), pp. 688-699.

Pedroso, M.D, Nascimento, C.B., Tusset, A.M., and Kaster, M.S. (2013). Performance Comparison between Nonlinear and Linear Controllers applied to a Buck Converter using Poles Placement Design. In: *15th European Conference on Power Electronics and Applications,* Lille, France, pp. 1-10, 2013.

Pedroso, M.D., Nascimento, C.B., Tusset, A.M., and Kaster, M.S. (2013). Performance Comparison Between Nonlinear And Linear Controllers With Weighted Adaptive Control Applied To A Buck Converter Using Poles Placement Design. In: *2013 IEEE International Symposium on Industrial Eelctronics*, Taipei, Taiwan, pp. 1-6.

Pedroso, M.D., Nascimento, C.B., Tusset, A.M., and Kaster, M.S. (2013). A Hyperbolic Tangent Adaptive PID + LQR Control Applied to a Step-Down Converter using Poles Placement Design Implemented in FPGA. *Mathematical Problems in Engineering*, 2013, pp. 1-8.

Pitel, G.E., and Krein, P.T. (2009). Minimum-Time Transient Recovery for DC–DC Converters Using Raster Control Surfaces. *IEEE Transactions on Power Electronics*, 24(12), pp. 2692 – 2703.

Priewasser, R., Agostinelli, M., Unterrieder, C., Marsili, S., and Huemer, M. (2014). Modeling, Control, and Implementation of DC–DC Converters for Variable Frequency Operation. *IEEE Transactions on Power Electronics*, 29(1), pp. 287-301.

Rashid, M.H. (2009). *Power Electronics: Circuits, Devices, and Applications*. Pearson Education, Delhi, India.

Salam, Z., Taeed, F., and Ayob, S.M. (2011). Design and Implementation of a Single Input Fuzzy Logic Controller for Boost Converters. *Journal of Power Electronics*, 11(4), pp.542-550.

Saleem, O., Hasan, H., Khan, A., and Javaid, U. (2017). Adaptive Fuzzy-PD Tracking Controller for Optimal Visual-Servoing of Wheeled Mobile Robots. *Control Engineering and Applied Informatics*, 19(3), pp. 56-68.

Saleem, O., Omer, U. (2017). Synergistic Speed Control Strategy for PMDC Motor. In: *2017 20th Internatioanl Multi-topic Conference*, Lahore, Pakistan, pp. 1-6.

Saleem, O., Rizwan, M., and Ahmad, M. (2018). Augmented Linear Quadratic Tracker for Enhanced Output-Voltage Control of DC-DC Buck Converter. *Control Engineering and Applied Informatics*, 20(4) pp. 40-49.

Saleem, O., Abbas, F., Khan, M.A., Imtiaz, M.A., and Khalid, S. (2018). Adaptive Collaborative Position Control of a Tendon-Driven Robotic Finger. *Control Engineering and Applied Informatics*, 20(2), pp. 87-99.

Saleem, O., and Mahmood-ul-Hasan, K. (2018). Adaptive collaborative speed control of PMDC motor using hyperbolic secant functions and particle swarm optimization. *Turkish Journal of Electrical Engineering & Computer Sciences*, 26(3), pp. 1612-1622.

Salim, N.D., Derawi, D., Abdullah, S.S., Mazlan, S.A., and Zamzuri, H. (2014). PID Plus LQR Attitude Control for Hexarotor MAV in Indoor Environments. In: *2014 IEEE International Conference on Industrial Technology*, Busan, South Korea, pp. 85-90.

Seraji, H. (1998). A new class of non-linear PID controller with robotic applications. *Journal of Robotic Systems*, 15, pp. 161-181.

Seshagiri, S., Block, E., Larrea, I., and Soares, L. (2016). Optimal PID Design for Voltage Mode Control of DC-DC Buck Converters. In: *2016 IEEE Indian Control Conference*, Hyderabad, India, pp. 99-104.

Shang, W.W., Cong, S., Li, Z.X., and Jiang, S.L. (2009). Augmented Nonlinear PD Controller for a Redundantly Actuated Parallel Manipulator. *Advanced Robotics*, 23(12-13), pp. 1725-1742.

Sun, L., and Gan, J. (2010). Researching of Two-Wheeled Self-Balancing Robot Base on LQR Combined with PID. In: *2010 2nd International Workshop on Intelligent Systems and Applications*, Wuhan, China, pp. 1-5.

Taha, W., Beig, A.R., and Boiko, I. (2018). Quasi Optimum PI Controller Tuning Rules for a Grid-Connected Three Phase AC to DC PWM Rectifier. *International Journal of Electrical Power & Energy Systems*, 96, pp. 74-85.

Tahri, F., Tahri, A., Allali, A., and Flazi, S. (2012). The Digital Self-Tuning Control of a Step Down DC-DC Converter. *Acta Polytechnica Hungarica*, 9(6), pp. 49-64.

Utkin, V., and Lee, H. (2006). Chattering Problem in Sliding Mode Control Systems. In: *International Workshop on Variable Structure Systems*, Alghero, Sardinia, Italy, pp. 346-350.

Vijayakumar, K., and Manigandan, T. (2016). Nonlinear PID Controller Parameter Optimization using Enhanced Genetic Algorithm for Nonlinear Control System. *Control Engineering and Applied Informatics*, 18(2), pp. 3-10.

Yaseen, M.H.A. (2017). A Comparative Study of Stabilizing Control of a Planer Electromagnetic Levitation using PID and LQR Controllers. Results in Physics, 7, pp. 4379-4387.

Zhang, X., Xu, J., Wu, J., Bao, B., Zhou, G., and Zhang, K. (2017). Reduced-Order Mapping and Design-Oriented Instability for Constant On-Time Current-Mode Controlled Buck Converters with a PI Compensator. *Journal of Power Electronics*, 17(5), pp.1298-1307.